

## Structural MRI Biomarkers for Preclinical and Mild Alzheimer's Disease

Christine Fennema-Notestine,<sup>1,2\*</sup> Donald J. Hagler Jr.,<sup>2</sup> Linda K. McEvoy,<sup>2</sup> Adam S. Fleisher,<sup>3</sup> Elaine H. Wu,<sup>2</sup> David S. Karow,<sup>2</sup> Anders M. Dale,<sup>2,3</sup> and the Alzheimer's Disease Neuroimaging Initiative

<sup>1</sup>Department of Psychiatry, University of California, San Diego, La Jolla, California

<sup>2</sup>Department of Radiology, University of California, San Diego, La Jolla, California

<sup>3</sup>Department of Neurosciences, University of California, San Diego, La Jolla, California



**Abstract:** Noninvasive MRI biomarkers for Alzheimer's disease (AD) may enable earlier clinical diagnosis and the monitoring of therapeutic effectiveness. To assess potential neuroimaging biomarkers, the Alzheimer's Disease Neuroimaging Initiative is following normal controls (NC) and individuals with mild cognitive impairment (MCI) or AD. We applied high-throughput image analyses procedures to these data to demonstrate the feasibility of detecting subtle structural changes in prodromal AD. Raw DICOM scans (139 NC, 175 MCI, and 84 AD) were downloaded for analysis. Volumetric segmentation and cortical surface reconstruction produced continuous cortical surface maps and region-of-interest (ROI) measures. The MCI cohort was subdivided into single- (SMCI) and multiple-domain MCI (MMCI) based on neuropsychological performance. Repeated measures analyses of covariance were used to examine group and hemispheric effects while controlling for age, sex, and, for volumetric measures, intracranial vault. ROI analyses showed group differences for ventricular, temporal, posterior and rostral anterior cingulate, posterior parietal, and frontal regions. SMCI and NC differed within temporal, rostral posterior cingulate, inferior parietal, precuneus, and caudal midfrontal regions. With MMCI and AD, greater differences were evident in these regions and additional frontal and retrosplenial cortices; evidence for non-AD pathology in MMCI also was suggested. Mesial temporal right-dominant asymmetries were evident and did not interact with diagnosis. Our findings demonstrate that high-throughput methods provide numerous measures to detect subtle effects of prodromal AD, suggesting early and later stages of the preclinical state in this cross-sectional sample. These methods will enable a more complete longitudinal characterization and allow us to identify changes that are predictive of conversion to AD. *Hum Brain Mapp* 00:000–000, 2009. © 2009 Wiley-Liss, Inc.

**Key words:** MRI; Alzheimer's disease; mild cognitive impairment; morphometry; brain imaging



Data used in the preparation of this article were obtained from the Alzheimer's Disease Neuroimaging Initiative (ADNI) database ([www.loni.ucla.edu/ADNI](http://www.loni.ucla.edu/ADNI)). As such, the investigators within the ADNI contributed to the design and implementation of ADNI and/or provided data but did not participate in analysis or writing of this report. Complete listing of ADNI investigators available at [http://www.loni.ucla.edu/ADNI/Data/ADNI\\_Authorship\\_List.pdf](http://www.loni.ucla.edu/ADNI/Data/ADNI_Authorship_List.pdf).

Contract grant sponsor: National Center for Research Resources, National Institutes of Health, USA [Morphometry Biomedical Informatics Research Network (BIRN, <http://www.nbirn.net>)]; Contract grant number: U24 RR021382; Contract grant sponsor:

Alzheimer's Disease Neuroimaging Initiative (ADNI; NIH); Contract grant number: U01 AG024904.

\*Correspondence to: Christine Fennema-Notestine, UCSD School of Medicine, 9500 Gilman Dr #0841, La Jolla, CA 92093-0841. E-mail: [fennema@ucsd.edu](mailto:fennema@ucsd.edu)

Received for publication 22 April 2008; Revised 8 January 2009; Accepted 12 January 2009

DOI: 10.1002/hbm.20744

Published online in Wiley InterScience ([www.interscience.wiley.com](http://www.interscience.wiley.com)).

## INTRODUCTION

To facilitate the development of therapies aimed at preventing or delaying the progression of Alzheimer's disease (AD), research has focused on the search for a sensitive, noninvasive, in vivo biomarker that would enable earlier, more accurate clinical diagnosis, and aid in monitoring disease progression and the effectiveness of therapeutic intervention [Dubois et al., 2007; Frank et al., 2003; Galasko, 2005; Thal et al., 2006]. Neuroimaging measures hold promise for guiding treatment before the occurrence of significant functional impairment or irreversible neuronal damage [Mueller et al., 2005; Scheltens et al., 2002; Thal et al., 2006], and such measures may facilitate the identification of individuals at greater risk for developing AD, improve the discrimination of AD from other types of dementia, and provide greater statistical power in clinical trials, allowing for smaller sample sizes [Jack et al., 2003, 2004; Thal et al., 2006]. They may also allow for shorter treatment trials by identifying individuals with high likelihood of imminent conversion.

The need for neuroimaging biomarkers is the motivation behind the multisite Alzheimer's Disease Neuroimaging Initiative (ADNI), aimed at facilitating the scientific evaluation of neuroimaging and other biomarkers in the onset and progression of mild cognitive impairment (MCI) and AD [Mueller et al., 2005]. MCI participants are impaired on one or more standardized tests of cognitive function, with memory as one of the impaired domains; they demonstrate no associated functional impairment and do not meet criteria for clinical diagnosis of dementia [Petersen, 2004]. Such individuals are at increased risk of converting to AD, estimated at 10–15% per year, compared with 1–2% per year for cognitively intact elderly [Petersen, 2004], and neuropathological studies support the notion that amnesic MCI may be a transitional state between healthy aging and AD [Markesbery et al., 2006; Morris et al., 2001; Petersen et al., 2006]. Individuals with single-domain, amnesic MCI (SMCI) may reflect the earliest stage of prodromal AD, whereas those with multidomain MCI (MMCI) may represent a later disease state. MCI is, however, a heterogeneous disorder; some individuals remain stable, others convert to another type of dementia, and still others revert to normal cognitive status [Boyle et al., 2006; Jicha et al., 2006; Petersen et al., 2006]. Methods to facilitate the prediction of which MCI individuals are likely to convert to AD would aid clinical trials by allowing them to focus on those at most risk of imminent conversion.

Structural MRI may prove useful in assessing the prognosis of individuals with MCI by enabling earlier clinical diagnosis and predicting disease progression. Previous studies of AD have examined regions affected early in the neurodegenerative process, including mesial temporal and temporoparietal association areas, and have shown that early atrophy in these regions is followed by more extensive involvement of frontal and parietal regions, leaving primary and secondary sensory areas relatively spared

until late in the disease [Atiya et al., 2003; Braak and Braak, 1991; Braak et al., 2006; Smith, 2002; Thompson et al., 2003, 2007]. Consequently, studies in early AD and in those at risk for AD, such as individuals with MCI, have focused primarily on mesial temporal regions, demonstrating that hippocampal and entorhinal cortex typically are smaller than those measured in controls [Atiya et al., 2003; Bell-McGinty et al., 2005; Bobinski et al., 1999; Convit et al., 1997; Du et al., 2001; Jack et al., 1997; Juottonen et al., 1998, 1999; Killiany et al., 2002; Singh et al., 2006; Xu et al., 2000] and predictive of future conversion to AD [de Leon et al., 2004; den Heijer et al., 2006; de Toledo-Morrell et al., 2004; Jack et al., 1999, 2005; Killiany et al., 1993, 2002; Stoub et al., 2005]. The definitive classification and specificity of these changes to AD, particularly for the hippocampus, remain a challenge [van de Pol et al., 2006], thus, ongoing work continues to examine additional regions and patterns of regional changes [Hua et al., 2008; Karas et al., 2004; Seo et al., 2007; Singh et al., 2006; Thompson et al., 2007; Whitwell et al., 2008]. The cingulate cortex, for example, has been shown to exhibit changes in at-risk individuals [Hirao et al., 2006; Jones et al., 2006] and in those known to eventually convert to AD [Killiany et al., 2000], and recent work suggests that MMCI individuals may evidence thinner precuneus cortices relative to SMCI [Seo et al., 2007]. The ADNI provides a rich resource of relevant data for normal elderly controls (NC) and individuals with MCI or early AD [Mueller et al., 2005] to determine the regional atrophy pattern associated with early stages of the disease. Such patterns may prove useful in predicting disease progression and in distinguishing AD from other neurodegenerative disorders.

To be of practical value in clinical trials or medical treatment, quantification of regional atrophy must be efficient and accurate, resilient in the face of variable brain morphology, and robust to differences in scanner platforms. Ongoing development within the NIH/NCRR sponsored Morphometry Biomedical Informatics Research Network (mBIRN) and the ADNI have resulted in procedures for image acquisition, automated corrections, and image analysis methods that enable large, multisite clinical research studies. In this study, we employed volumetric segmentation [Fischl et al., 2002, 2004a] and cortical surface reconstruction and parcellation [Dale et al., 1999; Dale and Sereno, 1993; Fischl et al., 1999a, 2004b] techniques for each individual's brain, combining the advantages of regions-of-interest (ROI) approaches that allow examination of disease effects in specific regions with the advantages of voxel-based approaches, which allow greater exploitation of information obtained from all brain areas.

This study examined the pattern of neurodegeneration associated with SMCI, MMCI, and AD and the feasibility of applying these methods to a large subset of the ADNI baseline cohort to successfully combine data across multiple scanner platforms. The findings will reveal whether these methods are robust in the face of extensive neuroanatomical variability observed in AD, are sensitive enough

to reveal the subtle characterization of SMCI, and are able to reveal signs of progressive impairment in early versus later stages of prodromal AD in this cross-sectional sample.

## MATERIALS AND METHODS

Raw MRI, basic demographic data, and clinical neuropsychological data were downloaded from the publicly available ADNI database ([www.loni.ucla.edu/ADNI](http://www.loni.ucla.edu/ADNI)); all image processing and analyses were performed locally in the Multi-modal Imaging Laboratory at UCSD.

### Alzheimer's Disease Neuroimaging Initiative

Data used in the preparation of this article were obtained from the ADNI database ([www.loni.ucla.edu/ADNI](http://www.loni.ucla.edu/ADNI)). The ADNI was launched in 2003 by the National Institute on Aging (NIA), the National Institute of Biomedical Imaging and Bioengineering (NIBIB), the Food and Drug Administration (FDA), private pharmaceutical companies, and nonprofit organizations, as a \$60 million, 5-year public-private partnership. ADNI's goal is to test whether serial magnetic resonance imaging (MRI), positron emission tomography (PET), other biological markers, and clinical and neuropsychological assessment can be combined to measure the progression of MCI and early AD. Determination of sensitive and specific markers of very early AD progression is intended to aid researchers and clinicians to develop new treatments and monitor their effectiveness, as well as lessen the time and cost of clinical trials.

The Principal Investigator of this initiative is Michael W. Weiner, M.D., VA Medical Center and University of California–San Francisco. ADNI is the result of efforts of many coinvestigators from a broad range of academic institutions and private corporations. Subjects have been recruited from over 50 sites across the U.S. and Canada. ADNI's goal was to recruit 800 adults, ages 55–90, to participate in the research—~200 cognitively normal individuals to be followed for 3 years, 400 people with MCI to be followed for 3 years, and 200 people with early AD to be followed for 2 years (see [www.adni-info.org](http://www.adni-info.org)).

### Participants

ADNI eligibility criteria are described at [http://www.adni-info.org/index.php?option=com\\_content&task=view&id=9&Itemid=43](http://www.adni-info.org/index.php?option=com_content&task=view&id=9&Itemid=43). Briefly, subjects are 55–90 years of age, had an informant able to provide an independent evaluation of functioning, and spoke either English or Spanish. All subjects were willing and able to undergo all test procedures including neuroimaging and agreed to longitudinal follow-up. Specific psychoactive medications are excluded. General inclusion/exclusion criteria are as follows:

1. Normal subjects: Mini-Mental State Examination (MMSE) [Folstein et al., 1975] scores between 24 and

30 (inclusive), a CDR of 0, nondepressed, non-MCI, and nondemented.

2. MCI subjects: MMSE scores between 24 and 30 (inclusive; exceptions made on a case by case basis), a memory complaint, objective memory loss measured by education adjusted scores on Wechsler Memory Scale Logical Memory II, a CDR of 0.5, absence of significant levels of impairment in other cognitive domains, essentially preserved activities of daily living, and an absence of dementia.
3. Mild AD: MMSE scores between 20 and 26 (inclusive; exceptions made on a case by case basis), CDR of 0.5 or 1.0, and meets NINCDS/ADRDA criteria for probable AD.

For this study, we further subdivided the MCI cohort into single-domain, amnesic MCI (SMCI), and multidomain MCI (MMCI) based on neuropsychological performance. Using the mean and standard deviation of each neuropsychological test obtained from the entire normal cohort ( $n = 227$ ), scores were converted into Z-scores. MCI participants were classified as having MMCI if a Z-score on any nonmemory test was less than  $-2$ ; otherwise a classification of SMCI was given. Nonmemory tests included Clock Drawing, Clock Copying, the Boston Naming Test, Verbal Fluency, Digit Symbol Substitution, Digit Span Forwards and Backwards, and Trail-Making Test parts A and B.

The cohort in this study is described in Table I. The groups were not significantly different on age ( $F < 1.0$ ,  $P > 0.05$ ) but did differ in years of education ( $F = 3.0$ ,  $P < 0.01$ ). The AD group had significantly fewer years of education relative to the NC ( $P < 0.005$ ), SMCI ( $P < 0.005$ ), and MMCI ( $P < 0.05$ ) groups; NC, SMCI, and MMCI groups did not significantly differ from each other ( $t$ 's  $< 1$ ,  $p$ 's  $> 0.05$ ). Sex distribution across the groups differed significantly ( $\chi^2 = 9.3$ ,  $P < 0.05$ ); the MMCI group had significantly fewer females relative to all other groups. All groups were significantly different in terms of MMSE and CDR (all  $P < 0.001$ ), except that SMCI and MMCI groups did not differ on CDR status, as expected based on diagnostic status.

### Procedures

Raw DICOM MRI scans (including two T1-weighted volumes per case) were downloaded from the public ADNI site (<http://www.loni.ucla.edu/ADNI/Data/index.shtml>); these data were collected across a variety of scanners with protocols individualized for each scanner, as defined at <http://www.loni.ucla.edu/ADNI/Research/Cores/index.shtml>. The MRI protocols for the relevant manufacturer platforms were optimized within the ADNI study to maximize the scientific utility of the data and to ensure use of equivalent pulse sequences [Jack et al., 2008] (<http://www.loni.ucla.edu/ADNI/Research/Cores/index.shtml>); an example protocol for a Siemens Magnetom Sonata syngo MR 2004A is as follows: sagittal inversion prepared 3D T1-weighted gradient echo sequence (MP-RAGE or equivalent)

TABLE I. Cohort demographics

Group	<i>n</i>	Age	Education	Sex (%)	MMSE	CDR
NC	139	75.6 (5.0) 62.1–89.7	16.0 (3.0) 6–20	45 F	29.1 (1.0) 25–30	0.0 (0.0)
SMCI	79	75.3 (7.7) 55.2–89.4	16.2 (2.4) 10–20	41 F	27.6 (1.7) 24–30	0.5 (0.0)
MMCI	96	74.2 (7.2) 54.6–87.8	15.8 (3.0) 8–20	21 F	26.6 (1.7) 23–30	0.5 (0.0)
AD	84	75.0 (7.6) 56.5–87.9	14.8 (3.1) 4–20	39 F	23.5 (2.1) 18–27	0.75 (0.25) 0.5–1.0

Values for Age, Education, MMSE and CDR reflect the mean (standard deviation) and range.

with  $TI = 1,000$  ms,  $TR = 2,400$  ms,  $TE =$  minimum, flip angle =  $8^\circ$ , bandwidth 180 Hz/px,  $FOV = 240$  mm, matrix size =  $192 \times 192$ , 60 slices, and slice thickness 1.2 mm.

In our laboratory, these data were reviewed for quality, automatically corrected for spatial distortion because of gradient nonlinearity [Jovicich et al., 2006] and B1 field inhomogeneity [Sled et al., 1998], registered, and averaged to improve signal-to-noise. The reduction of site-specific distortion effects and normalization of inhomogeneities significantly improves the accuracy of morphometric analysis and permits detection of subtle changes [Jovicich et al., 2006]. Local quality control measures excluded 15 cases (3.6% of available baseline cases at that time) because of extreme white matter disease or atrophy (e.g., one case with extensive left temporal lobe loss such that the temporal horn of the lateral ventricle subsumed a large extent of the anterior temporal lobe); these cases are not included in Table I.

Using volumetric segmentation [Fischl et al., 2002, 2004a] and cortical surface reconstruction [Dale and Sereno, 1993; Dale et al., 1999; Fischl et al., 1999a, 2004b] methods based on the publicly available FreeSurfer software package, volumetric measures were created for hippocampus, amygdala, caudate, putamen, nucleus accumbens, thalamus, ventricles, and white matter (Fig. 1). The automated, fully 3D whole-brain segmentation procedure [Fischl et al., 2002, 2004a] uses a probabilistic atlas and applies a Bayesian classification rule to assign a neuroana-

tomical label to each voxel. The probability of a class at each point is computed as the probability that the given class appeared at that location in the training set, modulated by the probability of the surrounding configuration of labels in the six cardinal directions, times the likelihood of obtaining the subject-specific measured intensity value from that class. The atlas consists of a manually derived training set created by the Center for Morphometric Analysis (<http://www.cma.mgh.harvard.edu/>) from 40 non-ADNI subjects across the age range, including individuals with AD. This process required only qualitative review to ensure no technical failure of the application. The accuracy of this automated procedure has been shown to be comparable to that of manual labeling and sensitive to subtle brain changes in AD and normal aging [Fischl et al., 2002, 2004a]. In addition, estimated total cranial vault (eTIV) volume was calculated to control for differences in head size for volumetric measures [Buckner et al., 2004].

The cortical surface was reconstructed to measure thickness at each surface location, or vertex, using a semiautomated approach with submillimeter accuracy [Dale and Sereno, 1993; Dale et al., 1999; Fischl and Dale, 2000; Fischl et al., 1999a]. Continuous, high-resolution maps then allow visualization of average group thickness or differences between groups at each vertex (as in Figs. 2 and 3). The explicit reconstruction of the cortical surface is a complex procedure, including correction of intensity variations because of magnetic field inhomogeneities, creation of a

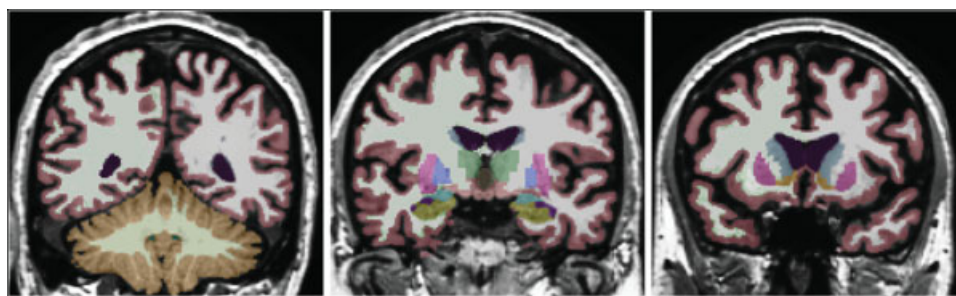
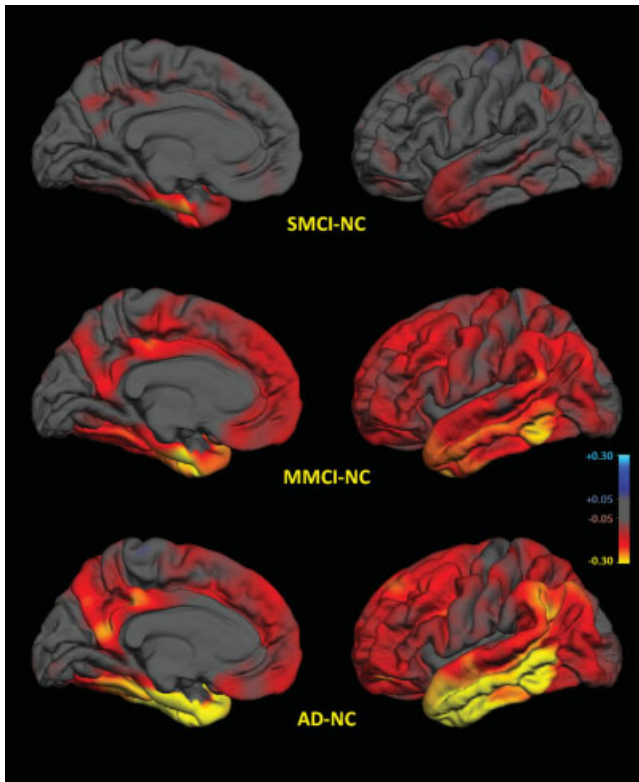


Figure 1.

Example coronal sections from FreeSurfer volumetric segmentation in an individual's native space to demonstrate regions-of-interest including hippocampus (gold), amygdala (sky blue), caudate (blue), putamen (pink), cerebellum (brown), nucleus accumbens (orange), body of the lateral ventricle and temporal horn of the lateral ventricle (purple).



**Figure 2.**

Group differences in average thickness (mm) for left hemisphere. Top row: NC vs. SMCI; middle row: NC vs. MMCI; bottom row: NC vs. AD. Left mesial views, right lateral views. The scale ranges from  $< -0.3$  (yellow) to  $> +0.3$  (cyan) mm thickness. Areas on the red-yellow spectrum indicate regions of thinning with disease: approximate color scale in mm is  $-0.05$  to  $-0.15$  dark red,  $-0.20$  bright red,  $-0.25$  orange, and  $< -0.30$  yellow. For thicker regions:  $+0.05$  to  $+0.15$  blue. Any differences smaller than  $\pm 0.05$  mm are gray.

normalized intensity image, and removal of the skull (non-brain) [Dale and Sereno, 1993; Dale et al., 1999; Fischl and Dale, 2000; Fischl et al., 1999a]. The resulting surface is covered with a polygonal tessellation and smoothed to reduce metric distortions. A refinement procedure is applied to obtain a representation of the gray/white boundary, and this surface is subsequently deformed outward to obtain an explicit representation of the pial surface. Once generated, the cortical surface model is manually reviewed and edited for technical accuracy. Minimal manual editing was performed in alignment with standard, objective editing rules. Each individual surface is non-rigidly aligned to an atlas in a spherical surface-based coordinate system [Fischl et al., 1999b] for continuous surface maps of average group thickness and group differences in average thickness, as well as for the application of the parcellation scheme described later. Studies demonstrate a high correlation of automatic and manual mea-

asures in vivo and ex vivo [Fischl and Dale, 2000; Fischl et al., 2002; Rosas et al., 2002].

The surface was then divided into distinct cortical ROIs [Fischl et al., 2004b]. In the spherical coordinate system, each surface location, or vertex, is assigned a neuroanatomical label based on (1) the probability of each label at each location in a surface-based atlas space, based on a manually parcellated training set; (2) local curvature information; and (3) contextual information, encoding spatial neighborhood relationships between labels. The resultant ROIs are then available within the subject-specific native space. The parcellation scheme [Desikan et al., 2006] labels cortical sulci and gyri, and thickness values are calculated in the numerous ROIs produced by this parcellation (Figs. 4 and 5). The labels for two cingulate regions were renamed within this study: the posterior and isthmus cingulate as defined in the original parcellation scheme [Desikan et al., 2006] are referred to here as the rostral - posterior cingulate and retrosplenial cortex, respectively. Thus, cortical thickness was averaged within numerous ROIs as well as estimated over continuous, high-resolution maps.

FreeSurfer image processing employed version 3.0.2 and used  $\sim 24$ -h computational time for image construction, using a dual quad core Intel(R) Xeon(R) CPU E5420 with a processing speed of 2.50 GHz and 16 GB ram. Use of several CPUs allowed processing of multiple subjects' scans to occur in parallel. Manual editing included correction of

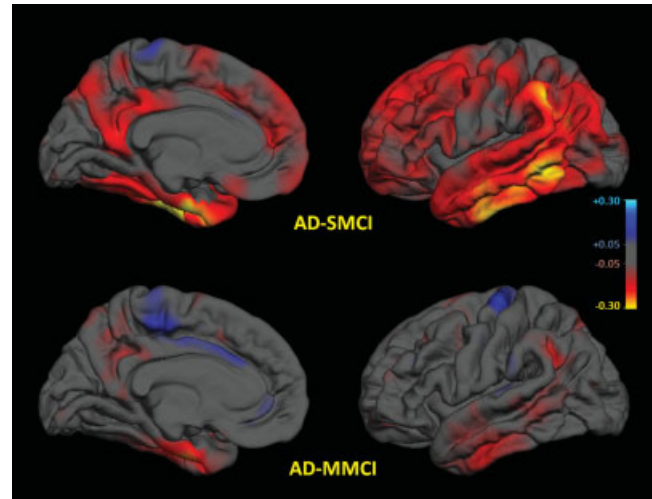


**Figure 3.**

Group differences in average thickness (mm) for left hemisphere. Top row: AD vs. SMCI; bottom row: AD vs. MMCI. Left mesial, right lateral views. The scale ranges from  $< -0.3$  (yellow) to  $> +0.3$  (cyan) mm thickness. Areas on the red-yellow spectrum indicate regions of thinning with disease: approximate color scale in mm is  $-0.05$  to  $-0.15$  dark red,  $-0.20$  bright red,  $-0.25$  orange, and  $< -0.30$  yellow. For thicker regions:  $+0.05$  to  $+0.15$  blue. Any differences smaller than  $\pm 0.05$  mm are gray.

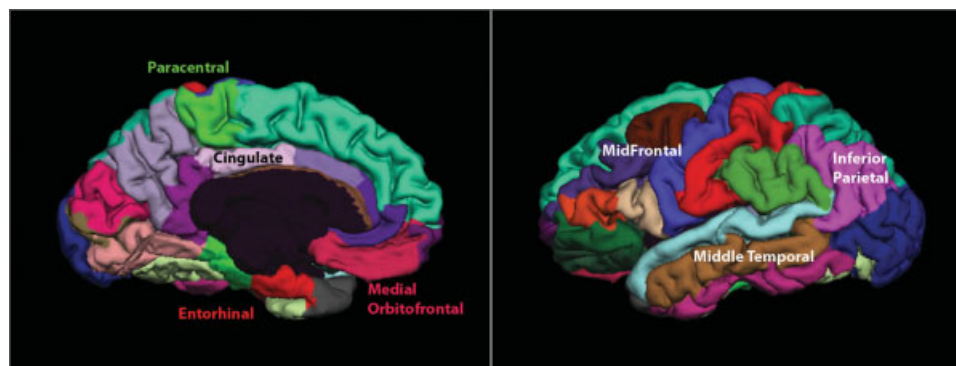


**Figure 4.**

Medial (left) and lateral (right) views of the cortical parcellation scheme. Regions-of-interest on the mesial surface include entorhinal cortex (red), four cingulate areas (shades of purple from retrosplenial, rostral posterior, caudal anterior, and rostral anterior), inferior parietal (violet). ROIs on the lateral surface include inferior (purple), middle (brown), and superior (light blue) temporal gyri, caudal (brown) and rostral (blue) midfrontal.

skull-stripping errors (e.g., removal of meninges), correction of the grey/white boundary to avoid inclusion of white matter lesions (appearing as hypointensities in the T1-weighted images) in thickness measurements, and other corrections routinely employed in FreeSurfer-based analyses; the implementation of these rules was overseen by an expert neuroanatomist (CFN). Qualitative review and editing described earlier required  $\sim 45$  min per subject.

### Statistical Analysis

Results include continuous maps representing group differences in average cortical thickness and ROIs for volumetric and thickness measures. Derived values for ROIs were submitted to repeated measures analyses of covariance (ANCOVAs), with covariates of age, gender, and, for volumetric measures, estimated total intracranial vault (eTIV) volume, to examine differences across all four groups; hemisphere was employed as a within-subject factor to assess left/right asymmetry across diagnostic groups. An  $\alpha$  of 0.001 was employed for group main effects. When a group effect was significant, subsequent pairwise contrasts were carried out, at the conventional  $\alpha = 0.05$  level, to assess significance of differences between individual groups in the predicted directions. Effect sizes were calculated for all regions using Cohen's  $d$  [Cohen, 1977], computed by dividing the mean difference between groups by the pooled standard deviation. Effect sizes and average percent differences were based on estimated marginal means resulting from the pairwise contrasts.

Planned comparisons characterize the extent to which temporal, posterior cingulate, and posterior parietal regions within each diagnostic group differ from the normal elderly control sample. Within each subject, principal regional measures include hippocampus, amygdala, entorhinal, parahippocampal, and lateral temporal cortices (lat-

eral inferior, middle, and superior temporal gyri); lateral, temporal horn, and third ventricles; four subdivisions of the cingulate cortex including retrosplenial (isthmus cortex), rostral posterior, caudal anterior, and rostral anterior); and precuneus, inferior, and superior parietal regions (Figs. 1 and 4). Based on the hypothesis that SMCI and MMCI may represent progressive stages of prodromal AD, SMCI and NC groups were expected to differ for mesial temporal and posterior cingulate regions, with even greater differences expected in MMCI and AD relative to NC. MMCI and AD groups were expected to exhibit thinner lateral temporal, parietal, and anterior cingulate cortices as pathology extends to association cortices with disease progression. Occipital, basal ganglia, and cerebellar regions were not expected to differ across groups. Additional exploratory analyses were performed to examine differences in frontal cortices (rostral and caudal midfrontal; medial and lateral orbitofrontal; superior regions; para-, pre-, and postcentral cortices); midfrontal and orbitofrontal cortices in particular may reflect vulnerability to AD pathogenesis prior to clinical diagnosis.

Finally, because significant group differences were apparent in multiple regions, even in the comparison of NC and SMCI groups, exploratory analyses were carried out to examine patterns of regional effects. Because of the unexpected findings in the MMCI group, as discussed in the Results section, we included only NC, SMCI, and AD participants in this exploration. To minimize multiple comparisons, these analyses were carried out only within left hemisphere for regions representing the expected path of AD-related changes, including: hippocampus and entorhinal cortex, rostral posterior cingulate and retrosplenial cortices, lateral middle temporal gyrus, inferior parietal cortex, medial orbitofrontal, and rostral midfrontal cortices. First, to suggest the hypothesized pattern of regional change that may occur with progression from NC to SMCI

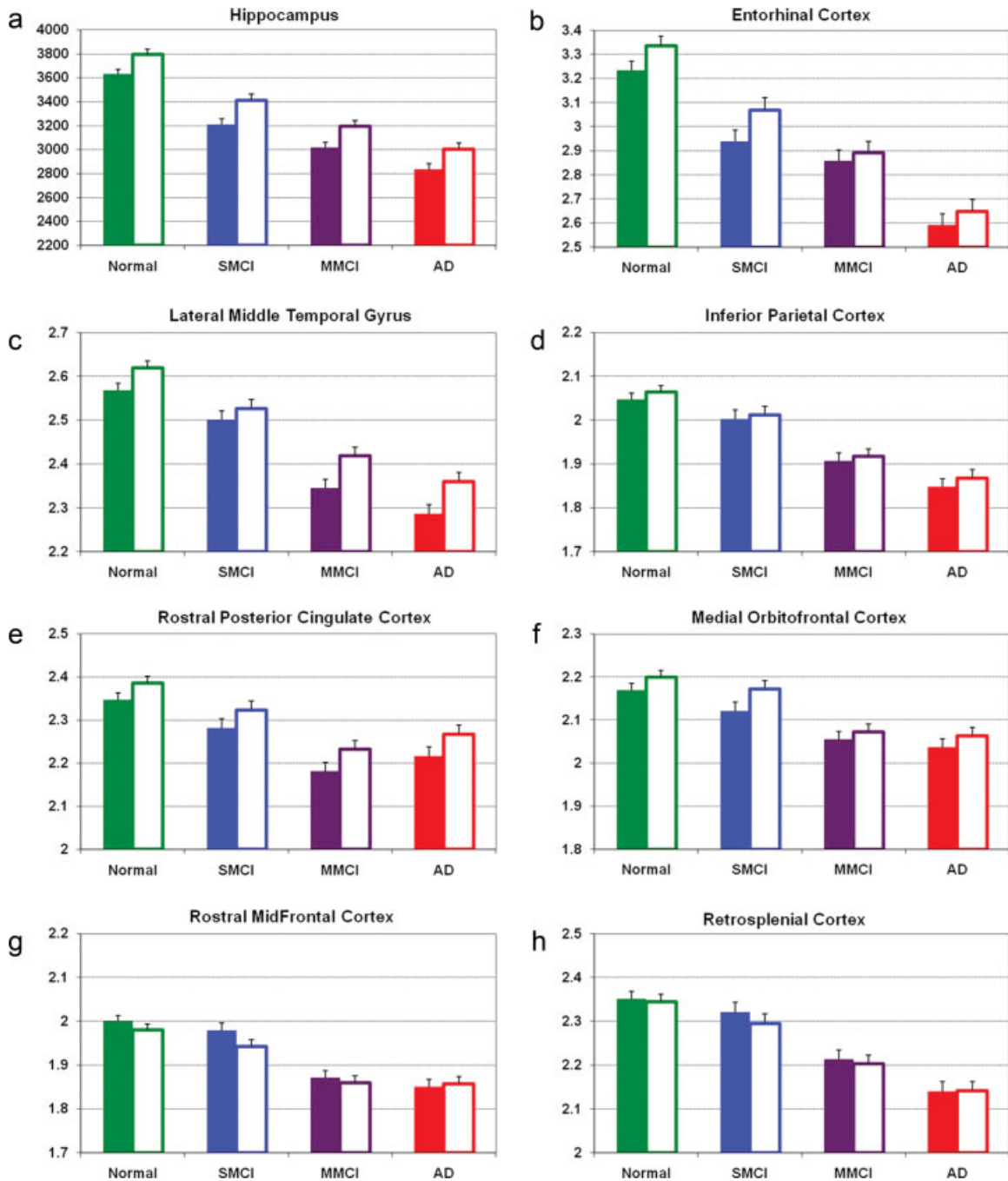


Figure 5.

Estimated marginal mean volume (mm<sup>3</sup>) for hippocampus and thickness (mm) for remaining regions by group for left hemisphere regions-of-interest accounting for sex and age effects. Significant group effects were present for all ROIs displayed. For a–e, all groups differed from each other. For medial orbitofrontal,

rostral midfrontal, and retrosplenial regions (f–h), NC and SMCI were significantly thicker relative to MMCI and AD; NC and SMCI were not different nor were MMCI and AD. Error bars = std. error of the mean. Solid bar = left hemisphere; outlined open bar = right hemisphere.

to AD, we examined the contribution of linear and quadratic components to a theoretical trajectory of change across these cross-sectional data. We performed an

ANCOVA with group as a factor and the standard covariates described earlier. Polynomial contrasts examined the significance of linear and quadratic effects. Linear progres-

sion would suggest a continuous, similar amount of atrophy between NC and SMCI as between SMCI and AD; a quadratic component would suggest a different degree of atrophy. That is, atrophy in a region with a significant negative quadratic component across groups might be accelerating with disease progression. Second, we examined group by region interactions through repeated measures ANCOVA with standard covariates; region was employed as a two-level, within-subject factor. Significant group by region interactions may suggest that cortical thinning occurs at a different rate in each region over disease progression.

## RESULTS

Comparisons of continuous cortical thickness maps provided a comprehensive view of group differences and support a pattern of progressive atrophy from NC to SMCI to MMCI to early AD. Differences in average thickness are displayed for each group relative to the NC group (Fig. 2); statistical analyses were performed on the ROI measures and are described in sections that follow. The surface maps suggest that the SMCI group averages were at least 250  $\mu\text{m}$  thinner in mesial temporal regions (orange/yellow) and 100–150  $\mu\text{m}$  thinner in the lateral temporal gyri (dark red). The MMCI group averages were similar to SMCI in the mesial temporal regions; however, relative to the NC group, the MMCI group was 250  $\mu\text{m}$  thinner in more extensive mesial and lateral temporal regions (orange/yellow), and 150  $\mu\text{m}$  thinner in posterior cingulate, inferior parietal, and midfrontal regions (red). Cortical thickness of NC and AD groups differed by more than 450  $\mu\text{m}$  in mesial temporal regions (yellow) and more than 200  $\mu\text{m}$  in posterior cingulate and temporoparietal association areas (red/orange/yellow); midfrontal regions were also thinner by 150  $\mu\text{m}$  (red). Each MCI subgroup also was compared with the AD group (Fig. 3) to support this apparent progression. As expected, the MMCI group was more similar to AD overall; that is, there were fewer differences in thickness. However, the maps demonstrated unanticipated trends toward thinner cortices in MMCI (by  $\sim 100$   $\mu\text{m}$  or more) relative to the AD group in anterior cingulate, paracentral, and precentral regions (Fig. 3, bottom row in blue). Statistical analyses were performed on the ROI data as follows.

### Region-of-Interest Group Comparisons

ROI analyses were performed across all groups, and these group effects are described here; the sections that follow detail regions affected by SMCI and MMCI specifically. Significant group effects were found for ventricular, temporal, posterior and rostral anterior cingulate, and posterior parietal ROIs ( $P$ 's  $< 0.001$ ); the group effect for caudal anterior cingulate did not reach significance ( $F(3,392) = 3.3$ ,  $P = 0.02$ ). Pairwise comparisons are presented in Table II, and estimated marginal means for several ROIs

are graphed in Figure 5, supporting the continuous thickness maps (Figs. 2 and 3). As expected, no significant group effects were demonstrated for the eTIV, cerebellar gray and white matter, caudate, putamen, cuneus, and pericalcarine regions (all  $F < 4.0$ ;  $P > 0.05$ ). Lateral occipital cortex and nucleus accumbens, however, were different across groups ( $F(3,392) = 11.9$ ,  $P < 0.001$ ;  $F(3,391) = 7.9$ ,  $P < 0.001$ , respectively).

Further exploratory investigations revealed significant group effects for all frontal ROIs ( $P$ 's  $< 0.001$ ), pre- ( $F(3,392) = 8.3$ ,  $P < 0.001$ ) and postcentral ( $F(3,392) = 9.5$ ,  $P = 0.001$ ) cortices, and a tendency for group differences in the paracentral ( $F(3,392) = 4.5$ ,  $P = 0.004$ ) region. Finally, the AD group tended to have less total volume of cerebral white matter ( $F(3,391) = 8.6$ ;  $P < 0.001$ ) and more white matter abnormalities (hypointensities on T1) ( $F(3,391) = 4.9$ ;  $P = 0.002$ ). For all regions with a significant overall effect of group, pairwise comparisons were performed; these are shown for each patient group relative to the NC group in Table II.

The investigation of hemispheric differences revealed right dominant asymmetries for hippocampal and entorhinal cortices with no significant group  $\times$  hemisphere interaction ( $F(1,391) = 4.0$ ;  $P < 0.05$ ;  $F(3,392) = 6.1$ ;  $P < 0.05$ , respectively). The body of the lateral ventricle was larger on the left than the right ( $F(1,391) = 10.2$ ,  $P < 0.005$ ), which tended to become more pronounced with degeneration ( $F(1,391) = 2.2$ ,  $P < 0.10$ ). Additional left dominant asymmetries were reported in volumetric measures of the putamen ( $F(1,391) = 6.7$ ,  $P = 0.01$ ) and white matter abnormalities ( $F(1,391) = 11.6$ ,  $P = 0.001$ ). Within the inferior temporal gyrus, no main effect of hemisphere was present, although there was a significant diagnosis by hemisphere interaction, suggesting a right dominant asymmetry with increasing degeneration ( $F(1,391) = 3.2$ ,  $P < 0.05$ ).

### Regions Affected in SMCI

Based on the hypothesis that SMCI and MMCI may represent early and later stages of prodromal AD, for the between-group comparisons gray matter volumes and cortical thickness measures were expected to be largest in the NC group, followed by SMCI, MMCI, and AD groups, in that order. Overall, the SMCI cohort evidenced smaller volumes and thinner cortices relative to NC in mesial and lateral temporal, fusiform, inferior parietal and precuneus, rostral posterior cingulate, and caudal midfrontal regions (Fig. 2, top row; Fig. 5; Table II). Pairwise comparisons and percent differences between SMCI and NC groups are presented in Table II, in the descending order of effect size for this comparison. All groups differed from each other for hippocampus (Fig. 5a), entorhinal cortex (Fig. 5b), amygdala, lateral middle (Fig. 5c) and inferior temporal gyri, banks of the superior temporal sulcus, and inferior parietal (Fig. 5d) cortices in the expected directions. NC individuals demonstrated significantly thicker



TABLE II. Pairwise comparisons for regions with a significant overall effect of group, in order of SMCI-NC comparison

ROI	Hemisphere	SMCI-NC				MMCI-NC				AD-NC			
		F	P	%Diff	Effect size	F	P	%Diff	Effect size	F	P	%Diff	Effect size
Hippocampus	Left	54.5	****	-11.8%	1.04	130.4	****	-17.3%	1.49	191.9	****	-22.0%	1.80
Hippocampus	Right	36.1	****	-10.2%	0.85	90.2	****	-15.8%	1.24	154.6	****	-21.0%	1.62
Entorhinal	Left	29.2	****	-9.1%	0.76	51.2	****	-11.6%	0.93	154.1	****	-19.6%	1.62
Amygdala	Left	24.6	****	-10.0%	0.70	66.3	****	-15.9%	1.07	122.7	****	-21.3%	1.44
Parahippocampal gyrus	Left	21.3	****	-8.6%	0.65	36.4	****	-10.6%	0.79	71.9	****	-15.0%	1.10
Entorhinal	Right	19.1	****	-8.0%	0.62	52.0	****	-12.8%	0.94	134.8	****	-20.5%	1.51
Amygdala	Right	15.2	****	-7.5%	0.55	64.8	****	-14.4%	1.05	97.7	****	-18.8%	1.29
Lateral middle temporal	Right	15.0	****	-6.3%	0.54	58.3	****	-7.7%	1.00	96.9	****	-9.8%	1.28
Parahippocampal gyrus	Right	14.5	****	-3.5%	0.54	26.6	****	-8.1%	0.67	37.1	****	-10.3%	0.79
Temporal horn	Right	11.7	****	20.5%	0.48	24.3	****	34.2%	0.64	57.2	****	59.6%	0.98
Fusiform	Left	11.2	***	-3.2%	0.47	61.0	****	-7.8%	1.02	86.0	****	-9.4%	1.21
Temporal pole	Left	11.2	***	-4.3%	0.47	39.0	****	-8.6%	0.82	41.6	****	-9.5%	0.84
Lateral middle temporal	Left	9.0	***	-2.6%	0.42	80.4	****	-8.9%	1.17	121.6	****	-10.9%	1.44
Temporal horn	Left	8.8	***	16.6%	0.42	29.4	****	35.2%	0.71	73.3	****	62.9%	1.12
Banks of the STS	Right	8.5	***	-3.8%	0.41	37.7	****	-8.1%	0.80	74.2	****	-11.4%	1.12
Lateral inferior temporal	Right	7.8	**	-2.7%	0.39	43.8	****	-7.0%	0.86	58.0	****	-8.4%	0.99
Lateral superior temporal	Right	7.7	**	-3.0%	0.39	43.6	****	-7.2%	0.86	41.3	****	-7.4%	0.84
Lateral superior temporal	Left	7.6	**	-2.8%	0.39	55.9	****	-8.1%	0.98	66.2	****	-8.8%	1.06
Lateral inferior temporal	Left	7.3	**	-2.6%	0.38	68.1	****	-8.2%	1.08	115.4	****	-10.8%	1.40
Banks of the STS	Left	7.3	**	-3.6%	0.38	43.5	****	-9.6%	0.86	77.5	****	-12.3%	1.15
Temporal pole	Right	7.3	**	-3.7%	0.38	29.5	****	-7.7%	0.71	52.4	****	-10.1%	0.94
Fusiform	Right	7.3	**	-2.6%	0.38	59.5	****	-7.9%	1.01	73.6	****	-9.0%	1.12
Precuneus	Right	6.9	**	-2.6%	0.37	31.8	****	-6.5%	0.74	45.8	****	-7.4%	0.65
Rostral posterior cingulate	Left	6.6	*	-2.7%	0.36	40.3	****	-7.2%	0.83	24.8	****	-5.4%	0.65
Inferior parietal	Right	6.3	*	-2.6%	0.35	41.3	****	-7.2%	0.84	70.3	****	-9.4%	1.09
Rostral posterior cingulate	Right	6.2	*	-2.6%	0.35	34.5	****	-6.5%	0.77	19.8	****	-4.9%	0.58
Caudal mid frontal	Right	6.0	*	-2.8%	0.34	32.5	****	-6.9%	0.74	39.2	****	-8.0%	0.82
Superior parietal	Left	5.2	*	-2.6%	0.32	13.4	****	-4.8%	0.48	28.6	****	-6.8%	0.70
Inferior parietal	Left	4.7	*	-2.2%	0.30	35.8	****	-7.2%	0.78	67.6	****	-9.6%	1.07
WM hypointensities	Left	4.6	*	23.0%	0.30	5.3	*	20.2%	0.30	13.7	****	44.2%	0.48
Caudal mid frontal	Left	4.4	*	-2.4%	0.29	36.0	****	-7.3%	0.78	53.3	****	-8.8%	0.95
Precuneus	Left	3.9	*	-2.1%	0.28	15.6	****	-5.0%	0.52	34.4	****	-8.8%	0.76
Cerebral white matter	Left	3.8	ns	-2.5%	0.27	8.7	***	-4.0%	0.39	20.6	****	-5.7%	0.59
Cerebral white matter	Right	3.8	ns	-2.3%	0.27	8.2	***	-3.7%	0.38	29.1	****	-6.4%	0.70
Medial orbitofrontal	Left	3.7	ns	-2.2%	0.27	23.0	****	-5.3%	0.63	27.7	****	-6.1%	0.68
Lateral occipital	Left	3.7	ns	-1.9%	0.27	13.5	****	-3.9%	0.48	23.4	****	-4.8%	0.63
Pars triangularis	Right	3.7	ns	-2.2%	0.27	21.2	****	-5.3%	0.60	11.8	****	-3.9%	0.45
Retrosplenial	Right	3.7	ns	-2.1%	0.27	26.5	****	-6.1%	0.67	60.0	****	-8.6%	1.01
Rostral mid frontal	Right	3.4	ns	-1.9%	0.26	34.7	****	-6.2%	0.77	34.7	****	-6.2%	0.77
Lateral ventricle	Left	3.3	ns	10.6%	0.26	23.5	****	28.4%	0.63	30.2	****	31.3%	0.72
Lateral orbitofrontal	Left	3.0	ns	-1.7%	0.24	35.4	****	-5.8%	0.78	36.2	****	-6.3%	0.78
Accumbens	Right	3.0	ns	-4.0%	0.24	13.1	****	-8.5%	0.47	16.5	****	-9.5%	0.53
Superior parietal	Right	2.7	ns	-1.8%	0.23	15.2	****	-4.8%	0.51	18.5	****	-5.7%	0.56
Lateral occipital	Right	2.5	ns	-1.5%	0.22	21.2	****	-4.8%	0.60	22.0	****	-5.0%	0.61
Superior frontal	Right	2.3	ns	-1.5%	0.21	31.4	****	-5.7%	0.73	33.9	****	-5.8%	0.76
WM hypointensities	Right	2.1	ns	13.7%	0.21	3.7	ns	18.0%	0.25	13.0	****	41.3%	0.47
Supramarginal	Right	2.0	ns	-1.5%	0.20	31.0	****	-6.3%	0.73	31.2	****	-6.6%	0.73
Lingual	Left	2.0	ns	-1.3%	0.20	16.0	****	-3.5%	0.52	18.6	****	-3.7%	0.56

TABLE II. (continued)

ROI	Hemisphere	SMCI-NC			MMCI-NC			AD-NC					
		F	P	%Diff	Effect size	F	P	%Diff	Effect size	F	P	%Diff	Effect size
Caudal anterior cingulate	Left	1.9	ns	-2.6%	0.19	6.1	*	-4.3%	0.32	0.2	ns	-0.8%	0.05
Superior frontal	Left	1.7	ns	-1.3%	0.19	30.9	*****	-5.6%	0.73	34.2	*****	-6.1%	0.76
Pars orbitalis	Right	1.7	ns	-1.6%	0.18	21.6	*****	-5.2%	0.61	9.1	***	-3.4%	0.39
Lingual	Right	1.5	ns	-1.1%	0.17	13.5	****	-3.2%	0.48	13.5	****	-3.2%	0.48
Medial orbitofrontal	Right	1.4	ns	-1.3%	0.17	29.1	*****	-5.9%	0.70	32.5	*****	-6.3%	0.74
Rostral anterior cingulate	Right	1.3	ns	-1.6%	0.16	24.3	*****	-6.8%	0.64	0.5	ns	-1.0%	0.09
Retrosplenial	Left	1.3	ns	-1.3%	0.16	25.1	*****	-5.9%	0.65	56.6	*****	-9.0%	0.98
Supramarginal	Left	1.3	ns	-1.2%	0.16	32.6	*****	-6.7%	0.75	38.2	*****	-7.2%	0.80
Paracentral	Left	1.2	ns	-1.6%	0.16	11.4	****	-4.9%	0.44	2.3	ns	-2.2%	0.20
Pars triangularis	Left	1.2	ns	-1.4%	0.15	31.6	*****	-6.9%	0.73	21.6	*****	-5.7%	0.61
Pars opercularis	Right	1.1	ns	-1.2%	0.15	15.4	****	-4.4%	0.51	14.6	****	-4.3%	0.50
Rostral mid frontal	Left	0.9	ns	-1.0%	0.14	37.2	*****	-6.6%	0.80	45.0	*****	-7.4%	0.87
Paracentral	Right	0.9	ns	-1.3%	0.13	9.7	***	-4.5%	0.41	2.2	ns	-2.1%	0.19
Rostral anterior cingulate	Left	0.7	ns	-1.2%	0.12	23.3	*****	-5.8%	0.63	6.7	*	-3.5%	0.34
Pars orbitalis	Left	0.7	ns	-1.0%	0.12	22.2	*****	-5.7%	0.62	18.2	*****	-5.4%	0.56
Lateral ventricle	Right	0.6	ns	4.6%	0.11	12.2	****	20.1%	0.46	23.8	*****	27.2%	0.63
Pars opercularis	Left	0.6	ns	-0.9%	0.11	22.8	*****	-5.6%	0.62	22.4	*****	-5.3%	0.62
Frontal pole	Right	0.6	ns	-1.1%	0.11	9.8	***	-4.7%	0.41	6.3	*	-3.5%	0.33
Frontal pole	Left	0.5	ns	-0.9%	0.10	17.4	*****	-5.8%	0.55	13.2	****	-5.1%	0.47
Accumbens	Left	0.4	ns	-2.3%	0.09	6.5	*	-8.8%	0.33	13.3	****	-12.1%	0.47
Precentral	Right	0.4	ns	-0.9%	0.09	15.1	****	-5.5%	0.51	7.8	**	-3.9%	0.36
Postcentral	Right	0.4	ns	-0.7%	0.08	13.9	****	-4.5%	0.49	14.0	****	-4.3%	0.49
Caudal anterior cingulate	Right	0.3	ns	0.7%	0.07	4.2	*	-3.0%	0.27	0.0	ns	-0.1%	0.01
Precentral	Left	0.1	ns	-0.6%	0.05	19.5	*****	-6.3%	0.58	9.1	***	-4.3%	0.39
Lateral orbitofrontal	Right	0.1	ns	-0.4%	0.05	25.6	*****	-5.0%	0.66	24.1	*****	-5.0%	0.64
Postcentral	Left	0.0	ns	-0.2%	0.02	11.6	****	-4.1%	0.44	19.0	*****	-4.8%	0.57
Third (3rd) ventricle	Left	0.0	ns	-0.2%	0.01	4.3	*	8.1%	0.27	12.0	****	13.9%	0.45

Regions are in order of descending effect size for the SMCI-NC comparison. The values and statistics reported here are based on the pairwise comparisons estimated marginal means, adjusted for age, sex and eTIV when relevant. The average percent difference in volume or cortical thickness between groups (- smaller; + larger) and the related effect size (Cohen's *d*) for the relevant group difference are reported. Level of significance for each comparison is indicated as follows: \*\*\*\*\* $P < 0.0001$ , \*\*\*\* $P < 0.001$ , \*\*\* $P < 0.005$ , \*\* $P < 0.01$ , \* $P < 0.05$ ; ns  $P > 0.05$ .

parahippocampal cortex relative to all groups; SMCI, MMCI, and AD groups were not different from each other for this region. MMCI, SMCI, and NC groups differed in the expected directions for the following regions: lateral superior temporal cortex, fusiform, temporal pole, rostral posterior cingulate (Fig. 5e), precuneus, and caudal midfrontal cortex; MMCI and AD were not significantly different for these same regions. Temporal horn of the lateral ventricle volume was significantly larger in SMCI relative to NC; SMCI and MMCI were both smaller relative to AD but not different from each other. SMCI did not demonstrate any significantly thicker regions relative to the NC group. In summary, the SMCI cohort distinguished itself from controls in temporal, fusiform, inferior parietal and precuneus, rostral posterior cingulate, caudal midfrontal, and temporal horn of the lateral ventricle measures (Fig. 2, top row; Fig. 5; Table II), while they were similar to MMCI in volume of the temporal horn of the lateral ventricle and similar to MMCI and AD in parahippocampal thickness. Remaining regions were not significantly different between NC and SMCI.

### Regions Affected in MMCI and AD

Overall, the MMCI cohort demonstrated additional regions of cortical thinning relative to NC and SMCI in lateral occipital, lingual, supramarginal, retrosplenial and anterior cingulate, frontal, and central cortices, alongside larger ventricles (Fig. 2, middle row; Table II). The MMCI reported effects in the frontal and central cortices were the results of exploratory analyses and were not expected to be detected in MMCI. The NC and SMCI groups differed from the MMCI and AD groups for lateral and third ventricle, lateral occipital, lingual gyrus, supramarginal gyrus, medial (Fig. 5f) and lateral orbitofrontal, rostral midfrontal (Fig. 5g), and superior frontal cortices, as well as the pars orbitalis, pars triangularis, pars operculum, frontal pole, pre-, and postcentral cortices. Retrosplenial cortex (Fig. 5h) was thinnest in AD and significantly thinner in MMCI relative to NC and SMCI. Finally, both MMCI and AD groups demonstrated thinner anterior cingulate cortices relative to NC and SMCI groups. Unexpectedly, the MMCI group demonstrated thinner rostral and caudal anterior cingulate, pre-, post-, and para-central cortices relative to all groups, including AD (MMCI vs. AD,  $P < 0.05$  for caudal anterior cingulate;  $P < 0.005$  for remaining regions; Fig. 3, bottom row—blue regions); the AD group was not significantly different from the NC or SMCI groups on paracentral, caudal anterior cingulate, or left rostral anterior cingulate. In summary, the MMCI cohort distinguished itself from NC and SMCI in lateral occipital, lingual, supramarginal, retrosplenial, anterior cingulate, frontal, and central cortices (Fig. 2, middle row) and lateral and third ventricular measures. MMCI differed from AD primarily in thicker retrosplenial cortex alongside unexpectedly thinner anterior cingulate, pre-, post-, and paracentral cortices (Fig. 3, bottom row—blue regions).

### Relative Effect Size of ROIs at Different “Stages” of Disease

Presupposing that SMCI individuals may represent the earliest stages of AD, there is great interest in identifying regions that may be most sensitive to these early changes. The regions that differed between NC and SMCI included numerous temporal cortices, the temporal horn of the lateral ventricle, rostral posterior cingulate, and several parietal and frontal regions. Pairwise effect sizes and percent differences for these regions are shown in Table II, supporting the potential use of the bilateral hippocampi, bilateral entorhinal, left amygdala, and left parahippocampal measures in differentiating NC and SMCI. The regions with the largest effect size in the SMCI-NC group comparison included the hippocampus and entorhinal cortex; these regions were on average 10% smaller relative to the NC group, alongside a greater than 15% increase in temporal horn volume. In MMCI, the difference relative to the NC group was greater in these regions, and the lateral inferior, middle, and superior temporal gyri and fusiform cortices demonstrated large effect sizes as well. In the comparison of NC and AD, the effect size for these same regions increased further, alongside larger differences for inferior parietal, banks of the superior temporal sulcus, retrosplenial, and some midfrontal regions. With a clinical diagnosis of AD, the percent difference from the NC group was approximately double that of the difference in SMCI for mesial temporal regions and nearly four times greater for left hemisphere lateral temporal and inferior parietal regions.

### Hypothesized Trajectories of Regional Atrophy With Disease Progression

To further explore the hypothesized regional changes that may occur with progression from NC to SMCI to AD, we examined the contribution of linear and quadratic components to a theoretical trajectory of change across these cross-sectional data. We excluded the MMCI group because of unexpected findings described earlier and focused on a subset of regions along the typical path of AD progression. The mesial temporal regions, including the entorhinal cortex and hippocampus, demonstrated only a significant negative linear effect across groups ( $P < 0.001$ ); other negative linear trajectories included the rostral posterior cingulate and medial orbitofrontal cortices ( $P < 0.001$ ). Regions with a significant negative quadratic component included lateral middle temporal gyrus, retrosplenial, inferior parietal ( $P < 0.05$ ), and rostral midfrontal cortices ( $P < 0.005$ ); these regions demonstrated a steeper negative slope between SMCI and AD than between NC and SMCI, suggestive of a greater acceleration of degeneration “later” in the disease.

Significant group  $\times$  region interactions supported a larger difference between groups (or a steeper slope) for the entorhinal cortex relative to the rostral posterior cingu-

late ( $F(2,297) = 39.1, P < 0.001$ ) and medial orbitofrontal cortex ( $F(2,297) = 40.5, P < 0.001$ ). There was no significant interaction for rostral posterior cingulate and medial orbitofrontal cortex ( $F(2,297) < 1.0, P > 0.05$ ) supporting a similar trajectory.

A significant group  $\times$  region interaction suggested a larger difference, or steeper slope, between groups for the lateral middle temporal gyrus, particularly between NC and SMCI, relative to the retrosplenial ( $F(2,297) = 3.2, P < 0.05$ ), inferior parietal cortex ( $F(2,297) = 9.1, P < 0.001$ ), and rostral middle frontal cortex ( $F(2,297) = 18.4, P < 0.001$ ). There was no significant interaction for retrosplenial and inferior parietal ( $F(2,297) < 1.0, P > 0.05$ ). There was a trend for an interaction between the inferior parietal and rostral midfrontal cortices ( $F(2,297) < 3.0, P = 0.05$ ), suggestive of a steeper trajectory between groups in the inferior parietal cortex.

## DISCUSSION

These findings demonstrate the feasibility of applying these mBIRN and ADNI supported high-throughput image analysis procedures for combining data from a variety of different scanner platforms and measuring numerous regions within each individual. These methods were robust in the face of extensive neuroanatomical variability observed in AD, revealed the expected characterization of AD, and detected subtle effects in SMCI and MMCI that may represent prodromal AD. ROI findings confirm and extend previous work in AD, demonstrating smaller white matter volumes, increased ventricular volumes and abnormal signal in the white matter, smaller hippocampal and amygdala volumes, and thinner temporal, parietal, cingulate, and frontal cortices compared with NC [e.g. Atiya et al., 2003; Singh et al., 2006; Thompson et al., 2003]. Although significant mesial temporal atrophy characterized all groups investigated here, including SMCI, MMCI, and AD, loss was widespread and evident across the cortex even within the SMCI group. This comprehensive investigation suggests a theoretical trajectory of disease progression as measured in vivo that supports neuropathological findings and demonstrates potential evidence of non-AD pathology in the MMCI group. The resultant pattern of AD-related neurodegeneration may be useful to assess the prediction of conversion to AD.

The investigation of SMCI and MMCI groups in this cross-sectional design provides insight into a hypothesized trajectory of disease progression. SMCI individuals may represent the earliest clinically detectable stage of AD, and there is great interest in identifying regions that are most sensitive to these early changes. In this large sample, significant differences were found between NC and SMCI within temporal regions, rostral posterior cingulate, inferior parietal, precuneus, and caudal midfrontal cortices. The examination of effect sizes suggests that the critical regions distinguishing NC and SMCI lie in the mesial

temporal regions as expected, including bilateral hippocampus, bilateral entorhinal cortex, and left amygdala, as supported by recent work [Hua et al., 2008; Seo et al., 2007; Singh et al., 2006; Whitwell et al., 2008], suggesting that these regions may be the most sensitive to early AD-related changes. However, the finding that significant atrophy extends beyond these regions into posterior cingulate, parietal, and frontal regions shows that significant and widespread damage occurs before standard clinical measures can detect AD. The pattern of thinning in SMCI overlaps to some extent with recent findings [Seo et al., 2007], although this larger sample demonstrated greater thinning in medial parietal, lateral middle temporal, and anterior cingulate regions and powered significant differences from NC in numerous ROIs. The finding that damage is detectable outside the mesial temporal area even at the earliest stage also may prove useful in defining a pattern of degeneration that will enable discrimination of early-stage AD from other disorders that also impact mesial temporal regions.

Although the pattern of results broadly supports the view that MMCI may be a later stage of prodromal AD than SMCI, some of the structural changes observed here support that this group includes individuals with non-AD pathology. Relative to SMCI, the presumably later stage of MMCI showed greater atrophy in the inferior and lateral temporal lobe, and significantly thinner temporoparietal association cortices, retrosplenial, anterior cingulate, and other frontal regions; these findings were more widespread relative to previous work [Seo et al., 2007], perhaps because of a larger, more heterogeneous MMCI sample. The AD and MMCI groups were relatively similar, with greater differences in some parietal, retrosplenial, and frontal regions. However, unexpectedly, the MMCI group tended to demonstrate thinner cortices in anterior cingulate and paracentral regions, while these regions were relatively spared in MCI and AD within this sample as well as in previous neuroimaging and neuropathological studies [Atiya et al., 2003; Braak and Braak, 1991; Braak et al., 2006; Smith, 2002; Thompson et al., 2003, 2007]. Although this finding requires replication to ensure that it is neither spurious nor because of methodological error, such trends may be driven by the inclusion of individuals in the MMCI cohort with impairment resulting from as yet unknown etiologies [Meyer et al., 2005; Winblad et al., 2004], such as frontotemporal dementia, often characterized by more anterior than posterior cortical loss, including anterior cingulate deficits [Boccardi et al., 2005]. The observed effect on motor regions may be related to other disorders such as Lewy body disease, often difficult to discern early in the stages of AD [Ballmaier and Memo, 2005; Ballmaier et al., 2004; McKeith et al., 2005]. Investigation of the neuropsychological profiles, to examine motor and executive function performance, and additional PET neuroimaging data are underway within the MMCI cohort.

We further explored the potential progression from NC to SMCI to AD, given the unexpected findings with the

MMCI cohort. These explorations suggest a theoretical trajectory of change that may occur with disease progression, and propose a pattern of regional change to be examined in subsequent within-subject, longitudinal investigations. As expected, the earliest and most dramatic effects across groups lie within the entorhinal cortex. Subsequently, rostral posterior cingulate is reduced similarly across groups. Other temporal and parietal regions, although thinner in SMCI, appear to be affected later to a greater extent, while thinning accelerates in the retrosplenial and numerous frontal regions. Considering some of these later changing regions, the lateral middle temporal gyrus may change most rapidly, followed by the posterior cingulate and inferior parietal cortices, and then the rostral middle frontal region. One proposed sequence of change, then, supports previous neuropathological findings as degeneration begins in the entorhinal cortex, moves through rostral posterior cingulate and medial orbitofrontal cortices, followed by lateral temporal, retrosplenial, and inferior parietal regions, and, subsequently, mid frontal cortex.

Finally, building on findings in AD both cross-sectional and longitudinal [e.g. Karas et al., 2003 Thompson, 2003, 12574429], recent work in MCI has suggested that left hemisphere regions may be more affected than the right [Seo et al., 2007], although there are conflicting reports across studies [Karas et al., 2004]. Our ROI-based exploration of hemispheric asymmetry supported strong right dominant asymmetries in the hippocampal and entorhinal cortices alongside left dominant asymmetries of the body of the lateral ventricle and the amount of white matter abnormalities; these asymmetries did not interact with diagnostic group. The mesial temporal asymmetries fit with previous findings of asymmetry in NC [e.g., Fennema-Notestine et al., 2007; Pedraza et al., 2004], while the ventricular and white matter asymmetries may be novel. Only the lateral measure of the inferior temporal gyrus demonstrated a significant group by hemisphere interaction, suggesting a right dominant asymmetry with increasing degeneration. These findings suggest that normal asymmetries in mesial temporal areas may not be affected by disease state, whereas lateral inferior temporal asymmetries may increase with progression. This study is potentially limited by the fact that we employed an existing probabilistic atlas that was not derived from these data. Longitudinal examination of modifications in asymmetry are critical to clarify this issue, given reports of changes in asymmetry in individuals at elevated risk for and diagnosed with AD [Barnes et al., 2005; Soininen et al., 1995].

## CONCLUSIONS

These cross-sectional findings provide direction for future studies of prodromal AD poised to determine whether changes in these regions are predictive of conversion to AD. The ADNI is following these same individuals over time and providing additional data measuring metab-

olism, neuropsychological performance, CSF markers, and genetics. Longitudinal morphometric analyses of these data are underway that may provide standardized predictive imaging biomarkers for AD. When combined with methods such as those described here, this will enable a more complete characterization of functional and anatomical changes associated with disease progression. The mBIRN and ADNI methods enabled sensitive quantification of widespread regional atrophy within individuals and across imaging platforms, providing the basis for the potential use of MRI biomarkers in large-scale clinical trials.

## ACKNOWLEDGMENTS

The authors thank Robin Jennings, Michele Perry, and Chris Pung for preprocessing data included in this study. Anders M. Dale is a founder and holds equity in CorTechs Labs, Inc, and also serves on the Scientific Advisory Board. The terms of this arrangement have been reviewed and approved by the University of California, San Diego in accordance with its conflict of interest policies. The ADNI [Principle Investigator: Michael Weiner] is funded by the National Institute on Aging, the National Institute of Biomedical Imaging and Bioengineering (NIBIB), and through generous contributions from the following: Pfizer Inc., Wyeth Research, Bristol-Myers Squibb, Eli Lilly and Company, GlaxoSmithKline, Merck & Co. Inc., AstraZeneca AB, Novartis Pharmaceuticals Corporation, Alzheimer's Association, Eisai Global Clinical Development, Elan Corporation plc, Forest Laboratories, and the Institute for the Study of Aging, with participation from the U.S. Food and Drug Administration. Industry partnerships are coordinated through the Foundation for the National Institutes of Health. The grantee organization is the Northern California Institute for Research and Education, and the study is coordinated by the Alzheimer's Disease Cooperative Study at the University of California, San Diego. ADNI data are disseminated by the Laboratory of Neuro Imaging at the University of California, Los Angeles.

## REFERENCES

- Atiya M, Hyman BT, Albert MS, Killiany R (2003): Structural magnetic resonance imaging in established and prodromal Alzheimer disease: A review. *Alzheimer Dis Assoc Disord* 17:177–195.
- Ballmaier M, Memo M (2005): Comparing gray matter loss profiles between dementia with Lewy bodies and Alzheimer's disease. *Funct Neurol* 20:69.
- Ballmaier M, O'Brien JT, Burton EJ, Thompson PM, Rex DE, Narr KL, McKeith IG, DeLuca H, Toga AW (2004): Comparing gray matter loss profiles between dementia with Lewy bodies and Alzheimer's disease using cortical pattern matching: Diagnosis and gender effects. *Neuroimage* 23:325–335.
- Barnes J, Scahill RI, Schott JM, Frost C, Rossor MN, Fox NC (2005): Does Alzheimer's disease affect hippocampal asymmetry? Evidence from a cross-sectional and longitudinal volumetric MRI study. *Dement Geriatr Cogn Disord* 19:338–344.

- Bell-McGinty S, Lopez OL, Meltzer CC, Scanlon JM, Whyte EM, Dekosky ST, Becker JT (2005): Differential cortical atrophy in subgroups of mild cognitive impairment. *Arch Neurol* 62:1393–1397.
- Bobinski M, de Leon MJ, Convit A, De Santi S, Wegiel J, Tarshish CY, Saint Louis LA, Wisniewski HM (1999): MRI of entorhinal cortex in mild Alzheimer's disease. *Lancet* 353:38–40.
- Boccardi M, Sabatelli F, Laakso MP, Testa C, Rossi R, Beltramello A, Soininen H, Frisoni GB (2005): Frontotemporal dementia as a neural system disease. *Neurobiol Aging* 26:37–44.
- Boyle PA, Wilson RS, Aggarwal NT, Tang Y, Bennett DA (2006): Mild cognitive impairment: Risk of Alzheimer disease and rate of cognitive decline. *Neurology* 67:441–445.
- Braak H, Braak E (1991): Neuropathological staging of Alzheimer-related changes. *Acta Neuropathol (Berl)* 82:239–259.
- Braak H, Alafuzoff I, Arzberger T, Kretschmar H, Del Tredici K (2006): Staging of Alzheimer disease-associated neurofibrillary pathology using paraffin sections and immunocytochemistry. *Acta Neuropathol (Berl)* 112:389–404.
- Buckner RL, Head D, Parker J, Fotenos AF, Marcus D, Morris JC, Snyder AZ (2004): A unified approach for morphometric and functional data analysis in young, old, and demented adults using automated atlas-based head size normalization: Reliability and validation against manual measurement of total intracranial volume. *Neuroimage* 23:724–738.
- Cohen J (1977): *Statistical Power Analysis for the Behavioral Sciences*. New York: Academic Press.
- Convit A, De Leon MJ, Tarshish C, De Santi S, Tsui W, Rusinek H, George A (1997): Specific hippocampal volume reductions in individuals at risk for Alzheimer's disease. *Neurobiol Aging* 18:131–138.
- Dale AM, Sereno MI (1993): Improved localization of cortical activity by combining EEG and MEG with MRI cortical surface reconstruction: A linear approach. *J Cogn Neurosci* 5:162–176.
- Dale AM, Fischl B, Sereno MI (1999): Cortical surface-based analysis. I. Segmentation and surface reconstruction *Neuroimage* 9:179–194.
- de Leon MJ, DeSanti S, Zinkowski R, Mehta PD, Pratico D, Segal S, Clark C, Kerkman D, DeBernardis J, Li J, Lair L, Reisberg B, Tsui W, Rusinek H (2004): MRI and CSF studies in the early diagnosis of Alzheimer's disease. *J Intern Med* 256:205–223.
- den Heijer T, Geerlings MI, Hoebeek FE, Hofman A, Koudstaal PJ, Breteler MM (2006): Use of hippocampal and amygdalar volumes on magnetic resonance imaging to predict dementia in cognitively intact elderly people. *Arch Gen Psychiatry* 63:57–62.
- Desikan RS, Segonne F, Fischl B, Quinn BT, Dickerson BC, Blacker D, Buckner RL, Dale AM, Maguire RP, Hyman BT, Albert MS, Killiany RJ (2006): An automated labeling system for subdividing the human cerebral cortex on MRI scans into gyral based regions of interest. *Neuroimage* 31:968–980.
- DeToledo-Morrell L, Stoub TR, Bulgakova M, Wilson RS, Bennett DA, Leurgans S, Wu J, Turner DA (2004): MRI-derived entorhinal volume is a good predictor of conversion from MCI to AD. *Neurobiol Aging* 25:1197–1203.
- Du AT, Schuff N, Amend D, Laakso MP, Hsu YY, Jagust WJ, Yaffe K, Kramer JH, Reed B, Norman D, Chui HC, Weiner MW (2001): Magnetic resonance imaging of the entorhinal cortex and hippocampus in mild cognitive impairment and Alzheimer's disease. *J Neurol Neurosurg Psychiatry* 71:441–447.
- Dubois B, Feldman HH, Jacova C, Dekosky ST, Barberger-Gateau P, Cummings J, Delacourte A, Galasko D, Gauthier S, Jicha G, Meguro K, O'Brien J, Pasquier F, Robert P, Rossor M, Salloway S, Stern Y, Visser PJ, Scheltens P (2007): Research criteria for the diagnosis of Alzheimer's disease: Revising the NINCDS-ADRDA criteria. *Lancet Neurol* 6:734–746.
- Fennema-Notestine C, Gamst AC, Quinn BT, Pacheco J, Jernigan TL, Thal L, Buckner R, Killiany R, Blacker D, Dale AM, Fischl B, Dickerson B, Gollub RL (2007): Feasibility of multi-site clinical structural neuroimaging studies of aging using legacy data. *Neuroinformatics* 5:235–245.
- Fischl B, Dale AM (2000): Measuring the thickness of the human cerebral cortex from magnetic resonance images. *Proc Natl Acad Sci USA* 97:11050–11055.
- Fischl B, Sereno MI, Dale AM (1999a): Cortical surface-based analysis. II. Inflation, flattening, and a surface-based coordinate system. *Neuroimage* 9:195–207.
- Fischl B, Sereno MI, Tootell RB, Dale AM (1999b): High-resolution intersubject averaging and a coordinate system for the cortical surface. *Hum Brain Mapp* 8:272–284.
- Fischl B, Salat DH, Busa E, Albert M, Dieterich M, Haselgrove C, van der Kouwe A, Killiany R, Kennedy D, Klaveness S, Montillo A, Makris N, Rosen B, Dale AM (2002): Whole brain segmentation: Automated labeling of neuroanatomical structures in the human brain. *Neuron* 33:341–355.
- Fischl B, Salat DH, van der Kouwe AJ, Makris N, Segonne F, Quinn BT, Dale AM (2004a): Sequence-independent segmentation of magnetic resonance images. *Neuroimage* 23(Suppl 1): S69–S84.
- Fischl B, van der Kouwe A, Destrieux C, Halgren E, Segonne F, Salat DH, Busa E, Seidman LJ, Goldstein J, Kennedy D, Caviness V, Makris N, Rosen B, Dale AM (2004b): Automatically parcellating the human cerebral cortex. *Cereb Cortex* 14:11–22.
- Folstein MF, Folstein SE, McHugh PR (1975): "Mini-mental state". A practical method for grading the cognitive state of patients for the clinician. *J Psychiatr Res* 12:189–198.
- Frank RA, Galasko D, Hampel H, Hardy J, de Leon MJ, Mehta PD, Rogers J, Siemers E, Trojanowski JQ (2003): Biological markers for therapeutic trials in Alzheimer's disease. Proceedings of the biological markers working group; NIA initiative on neuroimaging in Alzheimer's disease. *Neurobiol Aging* 24:521–536.
- Galasko D (2005): Biomarkers for Alzheimer's disease—clinical needs and application. *J Alzheimers Dis* 8:339–346.
- Hirao K, Ohnishi T, Matsuda H, Nemoto K, Hirata Y, Yamashita F, Asada T, Iwamoto T (2006): Functional interactions between entorhinal cortex and posterior cingulate cortex at the very early stage of Alzheimer's disease using brain perfusion single-photon emission computed tomography. *Nucl Med Commun* 27:151–156.
- Hua X, Leow AD, Parikshak N, Lee S, Chiang MC, Toga AW, Jack CR Jr, Weiner MW, Thompson PM (2008): Tensor-based morphometry as a neuroimaging biomarker for Alzheimer's disease: An MRI study of 676 AD, MCI, and normal subjects *Neuroimage* 43:458–469.
- Jack CR Jr, Petersen RC, Xu YC, Waring SC, O'Brien PC, Tangalos EG, Smith GE, Ivnik RJ, Kokmen E (1997): Medial temporal atrophy on MRI in normal aging and very mild Alzheimer's disease. *Neurology* 49:786–794.
- Jack CR Jr, Petersen RC, Xu YC, O'Brien PC, Smith GE, Ivnik RJ, Boeve BF, Waring SC, Tangalos EG, Kokmen E (1999): Prediction of AD with MRI-based hippocampal volume in mild cognitive impairment. *Neurology* 52:1397–1403.
- Jack CR Jr, Slomkowski M, Gracon S, Hoover TM, Felmlee JP, Stewart K, Xu Y, Shiung M, O'Brien PC, Cha R, Knopman D, Petersen RC (2003): MRI as a biomarker of disease progression in a therapeutic trial of milameline for AD. *Neurology* 60:253–260.

- Jack CR Jr, Shiung MM, Gunter JL, O'Brien PC, Weigand SD, Knopman DS, Boeve BF, Ivnik RJ, Smith GE, Cha RH, Tangalos EG, Petersen RC (2004): Comparison of different MRI brain atrophy rate measures with clinical disease progression in AD. *Neurology* 62:591–600.
- Jack CR Jr, Shiung MM, Weigand SD, O'Brien PC, Gunter JL, Boeve BF, Knopman DS, Smith GE, Ivnik RJ, Tangalos EG, Petersen RC (2005): Brain atrophy rates predict subsequent clinical conversion in normal elderly and amnesic MCI. *Neurology* 65:227–231.
- Jack CR Jr, Bernstein MA, Fox NC, Thompson P, Alexander G, Harvey D, Borowski B, Britson PJ, Whitwell LJ, Ward C, Dale AM, Felmlee JP, Gunter JL, Hill DL, Killiany R, Schuff N, Fox-Bosetti S, Lin C, Studholme C, DeCarli CS, Krueger G, Ward HA, Metzger GJ, Scott KT, Mallozzi R, Blezek D, Levy J, Debbs JP, Fleisher AS, Albert M, Green R, Bartzokis G, Glover G, Mugler J, Weiner MW (2008): The Alzheimer's Disease Neuroimaging Initiative (ADNI): MRI methods. *J Magn Reson Imaging* 27:685–691.
- Jicha GA, Petersen RC, Knopman DS, Boeve BF, Smith GE, Geda YE, Johnson KA, Cha R, Delucia MW, Braak H, Dickson DW, Parisi JE (2006): Argyrophilic grain disease in demented subjects presenting initially with amnesic mild cognitive impairment. *J Neuropathol Exp Neurol* 65:602–609.
- Jones BF, Barnes J, Uylings HB, Fox NC, Frost C, Witter MP, Scheltens P (2006): Differential Regional Atrophy of the Cingulate Gyrus in Alzheimer Disease: A Volumetric MRI Study. *Cereb Cortex* 16:1701–1708.
- Jovicich J, Czanner S, Greve D, Haley E, van der Kouwe A, Gollub R, Kennedy D, Schmitt F, Brown G, Macfall J, Fischl B, Dale A. (2006): Reliability in multi-site structural MRI studies: Effects of gradient non-linearity correction on phantom and human data. *Neuroimage* 30:436–443.
- Juottonen K, Laakso MP, Insausti R, Lehtovirta M, Pitkanen A, Partanen K, Soininen H (1998): Volumes of the entorhinal and perirhinal cortices in Alzheimer's disease. *Neurobiol Aging* 19:15–22.
- Juottonen K, Laakso MP, Partanen K, Soininen H (1999): Comparative MR analysis of the entorhinal cortex and hippocampus in diagnosing Alzheimer disease. *AJNR Am J Neuroradiol* 20:139–144.
- Karas GB, Burton EJ, Rombouts SA, van Schijndel RA, O'Brien JT, Scheltens P, McKeith IG, Williams D, Ballard C, Barkhof F (2003): A comprehensive study of gray matter loss in patients with Alzheimer's disease using optimized voxel-based morphology. *Neuroimage* 18:895–907.
- Karas GB, Scheltens P, Rombouts SA, Visser PJ, van Schijndel RA, Fox NC, Barkhof F (2004): Global and local gray matter loss in mild cognitive impairment and Alzheimer's disease. *Neuroimage* 23:708–716.
- Killiany RJ, Moss MB, Albert MS, Sandor T, Tieman J, Jolesz F (1993): Temporal lobe regions on magnetic resonance imaging identify patients with early Alzheimer's disease. *Arch Neurol* 50:949–954.
- Killiany RJ, Gomez-Isla T, Moss M, Kikinis R, Sandor T, Jolesz F, Tanzi R, Jones K, Hyman BT, Albert MS (2000): Use of structural magnetic resonance imaging to predict who will get Alzheimer's disease. *Ann Neurol* 47:430–439.
- Killiany RJ, Hyman BT, Gomez-Isla T, Moss MB, Kikinis R, Jolesz F, Tanzi R, Jones K, Albert MS (2002): MRI measures of entorhinal cortex vs hippocampus in preclinical AD. *Neurology* 58:1188–1196.
- Markesbery WR, Schmitt FA, Kryscio RJ, Davis DG, Smith CD, Wekstein DR (2006): Neuropathologic substrate of mild cognitive impairment. *Arch Neurol* 63:38–46.
- McKeith IG, Dickson DW, Lowe J, Emre M, O'Brien JT, Feldman H, Cummings J, Duda JE, Lippa C, Perry EK, Aarsland D, Arai H, Ballard CG, Boeve B, Burn DJ, Costa D, Del Ser T, Dubois B, Galasko D, Gauthier S, Goetz CG, Gomez-Tortosa E, Halliday G, Hansen LA, Hardy J, Iwatsubo T, Kalaria RN, Kaufer D, Kenny RA, Korczyn A, Kosaka K, Lee VM, Lees A, Litvan I, Londos E, Lopez OL, Minoshima S, Mizuno Y, Molina JA, Mukaetova-Ladinska EB, Pasquier F, Perry RH, Schulz JB, Trojanowski JQ, Yamada M (2005): Diagnosis and management of dementia with Lewy bodies: Third report of the DLB Consortium. *Neurology* 65:1863–1872.
- Meyer JS, Quach M, Thornby J, Chowdhury M, Huang J (2005): MRI identifies MCI subtypes: Vascular versus neurodegenerative. *J Neurol Sci* 229/230:121–129.
- Morris JC, Storandt M, Miller JP, McKeel DW, Price JL, Rubin EH, Berg L (2001): Mild cognitive impairment represents early-stage Alzheimer disease. *Arch Neurol* 58:397–405.
- Mueller SG, Weiner MW, Thal LJ, Petersen RC, Jack C, Jagust W, Trojanowski JQ, Toga AW, Beckett L (2005): The Alzheimer's disease neuroimaging initiative. *Neuroimaging Clin N Am* 15:869–877, xi-xii.
- Pedraza O, Bowers D, Gilmore R (2004): Asymmetry of the hippocampus and amygdala in MRI volumetric measurements of normal adults. *J Int Neuropsychol Soc* 10:664–678.
- Petersen RC (2004): Mild cognitive impairment as a diagnostic entity. *J Intern Med* 256:183–194.
- Petersen RC, Parisi JE, Dickson DW, Johnson KA, Knopman DS, Boeve BF, Jicha GA, Ivnik RJ, Smith GE, Tangalos EG, Braak H, Kokmen E (2006): Neuropathologic features of amnesic mild cognitive impairment. *Arch Neurol* 63:665–672.
- Rosas HD, Liu AK, Hersch S, Glessner M, Ferrante RJ, Salat DH, van der Kouwe A, Jenkins BG, Dale AM, Fischl B (2002): Regional and progressive thinning of the cortical ribbon in Huntington's disease. *Neurology* 58:695–701.
- Scheltens P, Fox N, Barkhof F, De Carli C (2002): Structural magnetic resonance imaging in the practical assessment of dementia: Beyond exclusion. *Lancet Neurol* 1:13–21.
- Seo SW, Im K, Lee JM, Kim YH, Kim ST, Kim SY, Yang DW, Kim SI, Cho YS, Na DL (2007): Cortical thickness in single- versus multiple-domain amnesic mild cognitive impairment. *Neuroimage* 36:289–297.
- Singh V, Chertkow H, Lerch JP, Evans AC, Dorr AE, Kabani NJ (2006): Spatial patterns of cortical thinning in mild cognitive impairment and Alzheimer's disease. *Brain* 129(Part 11):2885–2893.
- Sled JG, Zijdenbos AP, Evans AC (1998): A nonparametric method for automatic correction of intensity nonuniformity in MRI data. *IEEE Trans Med Imaging* 17:87–97.
- Smith AD (2002): Imaging the progression of Alzheimer pathology through the brain. *Proc Natl Acad Sci USA* 99:4135–4137.
- Soininen H, Partanen K, Pitkanen A, Hallikainen M, Hanninen T, Helisalmi S, Mannermaa A, Ryyanen M, Koivisto K, Riekkinen P Sr (1995): Decreased hippocampal volume asymmetry on MRIs in nondemented elderly subjects carrying the apolipoprotein E epsilon 4 allele. *Neurology* 45:391–392.
- Stoub TR, Bulgakova M, Leurgans S, Bennett DA, Fleischman D, Turner DA, DeToledo-Morrell L (2005): MRI predictors of risk of incident Alzheimer disease: A longitudinal study. *Neurology* 64:1520–1524.

- Thal LJ, Kantarci K, Reiman EM, Klunk WE, Weiner MW, Zetterberg H, Galasko D, Pratico D, Griffin S, Schenk D, Siemers E (2006): The role of biomarkers in clinical trials for Alzheimer disease. *Alzheimer Dis Assoc Disord* 20:6–15.
- Thompson PM, Hayashi KM, de Zubicaray G, Janke AL, Rose SE, Semple J, Herman D, Hong MS, Dittmer SS, Doddrell DM, Toga AW (2003): Dynamics of gray matter loss in Alzheimer's disease. *J Neurosci* 23:994–1005.
- Thompson PM, Hayashi KM, Dutton RA, Chiang MC, Leow AD, Sowell ER, De Zubicaray G, Becker JT, Lopez OL, Aizenstein HJ, Toga AW (2007): Tracking Alzheimer's disease. *Ann N Y Acad Sci* 1097:183–214.
- van de Pol LA, Hensel A, van der Flier WM, Visser PJ, Pijnenburg YA, Barkhof F, Gertz HJ, Scheltens P (2006): Hippocampal atrophy on MRI in frontotemporal lobar degeneration and Alzheimer's disease. *J Neurol Neurosurg Psychiatry* 77:439–442.
- Whitwell JL, Shiung MM, Przybelski SA, Weigand SD, Knopman DS, Boeve BF, Petersen RC, Jack CR Jr (2008): MRI patterns of atrophy associated with progression to AD in amnesic mild cognitive impairment. *Neurology* 70:512–520.
- Winblad B, Palmer K, Kivipelto M, Jelic V, Fratiglioni L, Wahlund LO, Nordberg A, Backman L, Albert M, Almkvist O, Arai H, Basun H, Blennow K, de Leon M, DeCarli C, Erkinjuntti T, Giacobini E, Graff C, Hardy J, Jack C, Jorm A, Ritchie K, van Duijn C, Visser P, Petersen RC (2004): Mild cognitive impairment—beyond controversies, towards a consensus: Report of the International Working Group on Mild Cognitive Impairment. *J Intern Med* 256:240–246.
- Xu Y, Jack CR Jr, O'Brien PC, Kokmen E, Smith GE, Ivnik RJ, Boeve BF, Tangalos RG, Petersen RC (2000): Usefulness of MRI measures of entorhinal cortex versus hippocampus in AD. *Neurology* 54:1760–1767.